

ON THE ROLE OF FLUID INFILTRATION ON BEDFORM EVOLUTION

Gerhard Bartzke¹, Lina Podszun¹ and Katrin Huhn¹

At present no general concept regarding key role of fluid infiltration on bedform evolution exists, basically because of difficulties in mapping the fluid stream in the vicinity of the sediment bed in a non-destructive way. Although numerous analogue wave tank or in-situ experiments provide high-resolution data, e.g., fluid profiles, there is still a clear lack in knowledge about the hydrodynamic conditions in the interior of bedforms particularly in-between single sediment grains. We generated a 3D numerical wave tank model using Smoothed Particle Hydrodynamics (SPH) to study the nature of flows near and in the interior of bedforms, as an alternative to the difficult task of in-situ measurements. With typical wave tank dimensions (i.e., $X = 2.5$ [m], $Y = 0.35$ [m], $Z = 0.8$ [m]), experiments were undertaken to test a simplified bedform geometry (stoss side slope = 13°) using a unimodal grain fraction. The water column was represented by 11 million fluid particles and the bedform by 480 immobile solid particles. A single solitary wave was introduced using a vertical paddle that accelerated to 0.8 [m/s] perpendicular to the bedform. During the entire simulation flow conditions above and in the interior of the bedform were monitored as a function of wave activity. Fluid velocities, extracted at each time step at each point of the tank, were used to determine free stream and inflow velocities, pore water flow track lines and residence time within the bedform. The results showed that inflow and pore water flow were evident in the bedforms and their flow directions appeared highly dependent on the location of the wave crest. In particular the development of a flow separation zone at the lee side of the bedform influenced the location of inflow into the bedform and thereby the flow direction within the pore spaces. This has been summarized in a new conceptual model for a better understanding of the hydrodynamic conditions in the interior of bedforms indicating the controlling effects of bed destabilization and bedform evolution.

Keywords: bedform; pore space flow; fluid infiltration; Smooth Particle Hydrodynamics (SPH)

INTRODUCTION

In the coastal environment, a great variety of bedform geometries exists, which occur on a wide number of spatial-temporal scales, owing to the textural variability of sediments and prevailing hydrodynamic drivers. Bedforms are important to sedimentologists because they are associated with certain kinds of hydrodynamic conditions, and to coastal engineers because they influence flow resistance and sediment transport dynamics (Coniglio et al., 2005).

The morphology of a bedform is mostly triangular with a fairly gentle upstream stoss slope and a steeper lee side slope (Julien, 1998). Bedform slopes at the stoss side typically range from 10° to 30° (Allen, 1970), whereas lee side slopes range from 15° to 30° (Bridge and Demicco, 2008). For the understanding of the generation of these different bedforms, various researchers focused their investigations predominantly on the morphology, the hydrodynamic conditions in the water column, and the related sediment transport dynamics (Bridge and Demicco, 2008; Leeder, 1999). For example, the hydrodynamic conditions above bedforms were studied extensively by investigating the flow in either unidirectional flows or under wave motion in various laboratory experiments or *in-situ* field measurements (e.g., (Baas, 1994; Bartzke et al., 2013; Best, 1992; Black and Paterson, 1997; Heald et al., 2004; Leeder, 1980; Mc Cave, 1984; Venditti and Bennett, 2000; Venditti et al., 2005)). Accordingly, at present the hydrodynamic conditions above bedforms are understood fairly well. It has been reviewed by Bennett and Best (1995) that on the stoss side the flow is accelerating over the bedform crest, whereas on the lee side of bedforms the well-known zone of flow separation develops. An overview of the governing processes dealing with hydrodynamic conditions and the related sediment dynamics of bedforms are provided by Venditti (2013).

Nevertheless, it is extremely difficult to measure fluid flow in the direct vicinity of the sediment surface or even in the shallow sediment bed with analogue laboratory sensors such as ADV's, which easily cause the sediment to scour (van Rijn, 1984), and eventually destroy the bed (Allen, 1970; Leeder, 1999). Consequently, it is problematic to quantify or even visualize the sediment transport processes that occur in the water column at the direct vicinity and particularly in the interior of bedforms at the same time.

¹MARUM, Universität Bremen, Leobener Straße, Bremen, D-28359, Germany

Numerical models have the capability to overcome these limitations of analogue experiments and can provide a powerful tool to visualize and quantify the hydrodynamic conditions in the interior of bedforms (Drake and Calantoni, 2001; Schmeeckle and Nelson, 2003). For example, the numerical technique Smoothed Particle Hydrodynamics (SPH) is capable to investigate the fluid flow conditions occurring at both the direct vicinity and in the interior of bedforms. Unlike most numerical methods, SPH does not need a mesh or grid to discretize the physical domain rather the fluid is discretized by a certain number of spherical, numerical “water” particles. This is an effective way to simulate different hydrodynamic processes and flow conditions respectively, i.e., laminar streaming, but also turbulences in a water body in three dimensions and all scales (Barreiro et al., 2013; Dalrymple and Rogers, 2006; Gomez-Gesteira et al., 2012). In addition, ‘grain sediment’ particles are similarly discretized by single solid particles with mass. Therewith, hydrodynamic conditions along different sediment bedforms could be simulated under different free-stream flow conditions.

The main goal of this study was to investigate inflow into simplified bedforms and to test a typical bedform geometry on the inflow characteristics, as well as pore water flow pattern. This ultimately could help to understand the nature of the inflow into the interior of a bedform and might give some implications for sediment destabilization and erosion.

METHODS

The numerical simulation technique Smooth Particle Hydrodynamics (SPH) was used to set up a 3D numerical wave tank model. SPH does not need a mesh or grid to discretize the physical domain to calculate the spatial derivatives of the fluid dynamical laws (Dalrymple and Rogers, 2006; Monaghan, 1992). In any SPH model, the physical domain is discretized by a finite number of numerical particles that interact with each other following the fluid conservation laws (Monaghan, 1992).

Thereby, each particle in an SPH model is assigned with its own physical properties such as mass, density, or pressure. In the case of a fluid, the physical integration between individual fluid particles is solved following a mesh less lagrangian model aiming at solving the Navier-Stokes equations through the convolution-based discretization (Dalrymple and Rogers, 2006). The derivatives are found by analytical differentiation of interpolation formulae (Gomez-Gesteira et al., 2012). By this calculation architecture, SPH is capable of simulating various flow features in a water body in three dimensions such as laminar streaming but also turbulences (Barreiro et al., 2013). A detailed review of the involved SPH algorithms exceeds the scope of this paper. However, a complete derivation of the numerical procedure such as the approximation of the flow equations by an integral interpolation in SPH models can be found in (e.g., (Barreiro et al., 2013; Crespo et al., 2008; Gomez-Gesteira et al., 2012; Monaghan, 1992; 1994; 2005)). The “dynamic boundary particle” technique was used to discretize the solid spherical particles. This technique is commonly applied in SPH models to simulate the interactions of fluid and solids (Gomez-Gesteira et al., 2012). Please refer to Gomez-Gesteira et al. (2012) or Barreiro et al. (2013) for further information about the boundary conditions in SPH.

In our experiments, we used the open-source 3D SPH model DualSPHysics (www.dualsphysics.org, version 3.1). The mathematical “correctness,” validation and applicability of DualSPHysics to investigate various scenarios has been shown by many prior studies (e.g., (Dalrymple and Rogers, 2006; Gomez-Gesteira et al., 2012; Monaghan, 1992)).

Model configuration

We generated a 3D numerical wave tank model using the SPH method to investigate the fluid flow conditions occurring at the direct vicinity and in the interior of bedforms. Please note that in this study, terms such as “bedforms”, “grains”, “sediment” or “inflow” are used, even though we recognize that the context is related to a numerical rather than a natural one. The same applies to the used SI units, which are clearly dimensionless and are, therefore, given in square brackets, respectively. All presented data were processed using programmed routines in Paraview 4.1 and Matlab 2013 environments.

A schematic of the 3D numerical wave tank is shown in Figure 1. The entire fluid model was generated out of more than 11 Million particles. Initially, a box opened to the top was created using five solid, un-deformable walls (Figure 1). Our 3D numerical model was generated in typical wave tank dimensions. The entire length of the front and back walls were 2.68 [m] ranging from 0.0 [m] to 2.68 [m]. Both sidewalls were created at the left $X = 0.0$ [m] and right $X = 2.68.0$ [m] ends of the wave tank and were 0.25 [m] wide, ranging from $Y = 0.0$ [m] to $Y = 0.2$ [m]. All back, front and sidewalls

were 0.8 [m] high. The size of the bottom wall of the tank ranged from $X = 0.0$ [m] to $X = 2.65$ [m] and from $Y = 0.0$ [m] to $Y = 0.25$ [m]. For the initiation of a wave the left sidewall was classified as a wave maker boundary condition (Barreiro et al., 2013; Gomez-Gesteira et al., 2012), being able to accelerate into the X direction 0.8 [m/s] perpendicular to the wave tank. The vertical paddle was allowed to move to $X = 0.3$ [m]. Note that the paddle was positioned directly into the wave tank so no fluid particles could leak through the sidewalls of the wave tank.

One flat bedform having a stoss side slope of 13° was generated as a representative for typical bedforms. The bedform was created at the bottom of the wave tank and ranged from $X = 0.5$ [m] to $X = 1.5$ [m], and was $Z = 0.15$ [m] high, and $Y = 0.25$ [m] wide, and was generated out of 480 solid spheres. Therefore, a simplified grain fraction ($D_{50} = 4000$ [μm]) was used, wherein all spheres were distributed randomly. Note, larger spheres were chosen compared to natural gravel for a high-resolution quantification of hydrodynamic processes that occur within the pore spaces to test this numerical approach. The average porosity in the bedform was $\Phi = [0.37]$. In order to allow numerical fluid flow in the pores a “void boundary condition” was used that classified the pore space between the spherical particles as void space. After the experiment was set up the wave tank was flooded with fluid particles to 0.35 [m] in height.

The entire simulation was stopped after $t = 1.8$ [s] when the wave crest reached the back wall. This procedure ensured that potential wave reflections caused by the back wall did not influence our model results. In total, the model is simulating $t = 1.8$ [s] real time and took 11.3 h calculation time per experimental run on an Intel Xeon E5 cluster and an installed NVidia Tesla K20c graphics card.

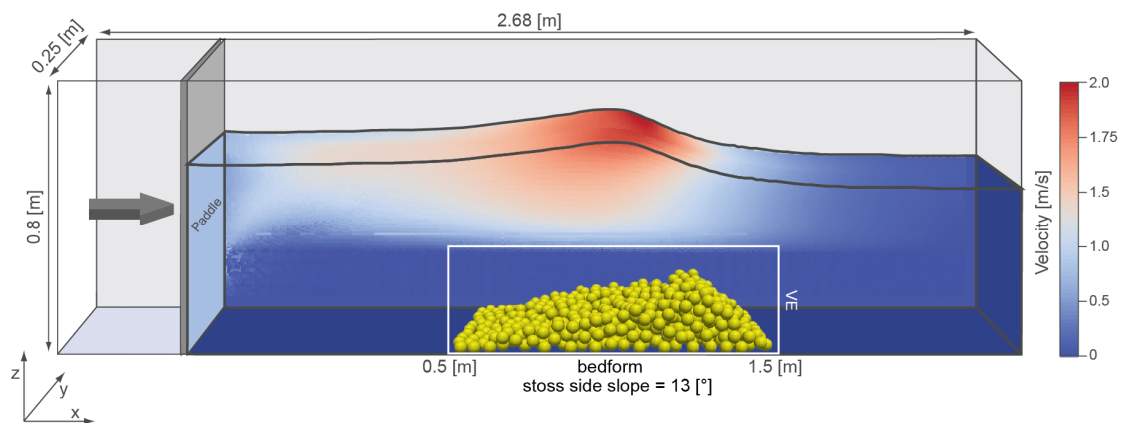


Figure 1. Schematic of the 3D numerical wave tank. An accelerating wave maker was implemented to generate a solitary wave. The white colored rectangle indicates the location of tested bedform, which is vertically extended (VE) or a better representation. The stoss side slope was 13° and the lee side slope was 38° .

Measurements and data statistics

During the entire simulation, the flow velocities and directions above and in the interior of the bedform were monitored as a function of wave activity and extracted at each model iteration step $t = 0.01$ [s]. This approach allowed a three-dimensional high-resolution analysis of the flow conditions in the water column as well as a measurement of potential flow variations in the direct vicinity and in the interior of the bedforms.

Four example cases were processed as a representative time series including $t_1 = 0.7$ [s], $t_2 = 0.95$ [s], $t_3 = 1.2$ [s] and $t_4 = 1.45$ [s]. At each time step, a vertical high-resolution cross-section cutting through the center of the bedform was analyzed along the entire wave tank. This XZ-plane ranged from $X = 0.5$ [m] to $X = 1.5$ [m] and $Z = 0.0$ [m] to $Z = 0.6$ [m] at $Y = 0.11$ [m]. The velocity data were color coded to highlight the flow pattern (Figure 2), whereas the velocity in X direction were rescaled from -0.06 [m/s] to 0.06 [m/s] to highlight variations within the pore spaces (Figure 3 A - D). Additionally, two zoom outs at $t_1 = 0.7$ [s] and $t_4 = 1.45$ [s] were generated for a high resolution representation of the flow directions and velocities near the lee side (Figure 3E and 3F). These zoom outs indicate the flow directions by three-dimensional glyphs, i.e., arrows. All arrows were color coded to illustrate the velocities in the X direction. Note that yellow colored spheres in Figures 2 - 6 indicate the locations of the cut spheres that are part of the bedform.

To provide a deeper insight of the flow evolution with respect to time in the interior of the bedforms, the pore water flow pattern presented in Figure 4A was calculated. In addition, the residence time of the fluid particle in the different pore spaces was calculated to quantify zones of high and low-fluid inflow activities, with respect to time (Figure 4B).

RESULTS

The results revealed an inflow into the bedform that propagated as a current throughout the pore spaces. Measurements above the bedform indicated the hydrodynamic conditions in the water column. The velocity distributions extracted from the interior of the bedform showed inflow into the pore spaces. Pore water flow pattern revealed the role of the flow throughout the pore spaces, whereby the flow residence times indicate locations of relatively low and high fluid flow in the specific parts of the bedform as a function of the wave location.

Free stream flow velocities in the water column

The velocity distribution of the wave as well as the wave shape characteristics are presented in Figure 2. In order to highlight general observations, the wave characteristics recorded at $t_2 = 0.95$ [s] of the experiment is described in detail as an example case (Figure 2B). At that time step, the wave crest was located at $X = 0.9$ [m] and $Z = 0.52$ [m], while the trough of the wave was positioned at $X = 1.35$ [m] and $Z = 0.42$ [m]. The measured amplitude was $Z = 0.17$ [m], where the wave slope was 11° at the upstream limb and 19° at the downstream limb indicating a slightly asymmetric pattern. When investigating the free stream flow velocities in the water column, relatively high-flow speeds were measured close to the wave crest. Velocities ranged from 0.6 to 1.0 [m/s] (yellow to bright red colors in Figure 2). Towards the bottom of the wave tank, the flow velocities decreased from 0.4 to 0.1 [m/s] (light blue colors in Figure 2). Interestingly, within the region below the wave crest, the measurements indicate a velocity decrease towards the vicinity of the bedform that was accompanied by a change in the pattern of the velocity distribution.

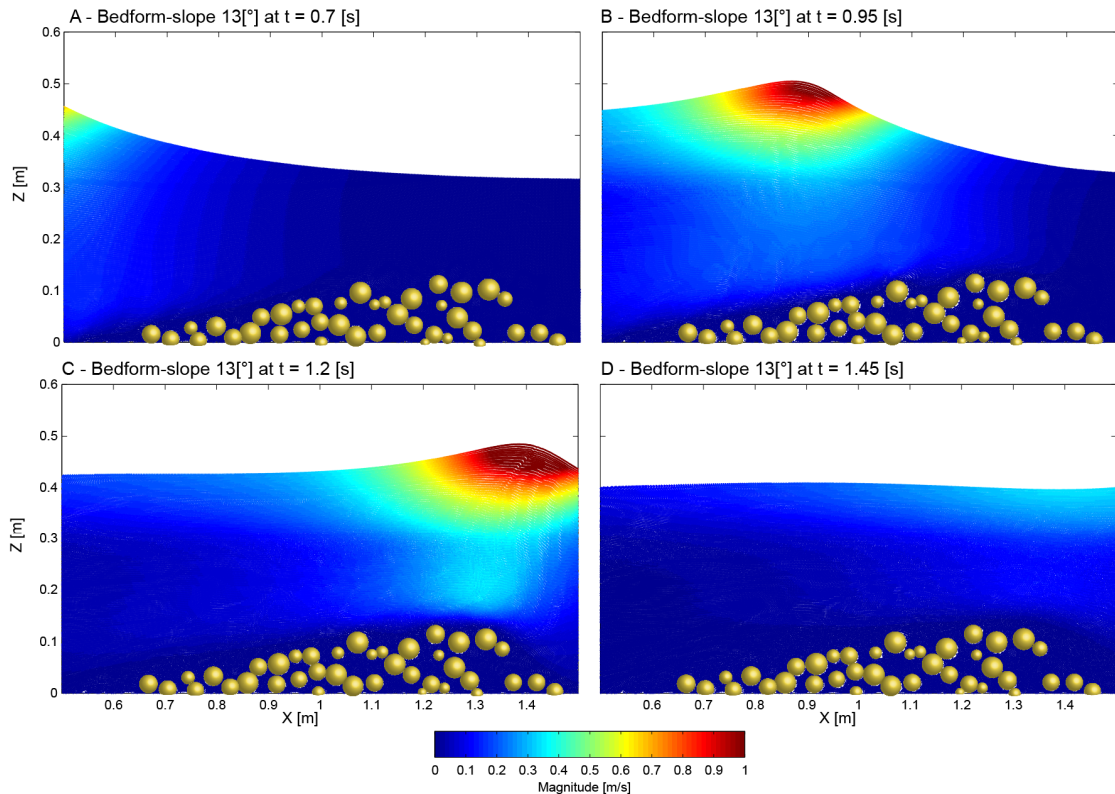


Figure 2. Overview of the X-Z slices cut at $Y = 0.11$ [m], demonstrating the velocity magnitudes measured in the water column with respect to wave crest position. The yellow colored spheres indicate the locations of the cut solid particles.

Inflow velocities and flow pattern through pore spaces in the bedform

With a focus on velocity ranges in the interior of the bedforms, X-Z velocity cutouts are presented at four representative time steps (Figure 3). The flow velocity measurements into the X direction indicate clear evidence that an inflow penetrated throughout the interior of the bedform with respect to time (bright red velocity patches in the interior of the bedform, Figure 3). In the case when the wave crest was located in front of the bedform at $t_1 = 0.7$ [s] relatively high velocities in the pore spaces of up to 0.04 [m/s] were measured in a shallow layer close to the stoss side of the bedform ranging from $X = 0.7$ [m] to $X = 1.2$ [m]. At $t_2 = 0.95$ [s] when the wave crest was located directly above the bedform the maximal downstream velocities of 0.06 [m/s] were measured in the center of the entire bedform ranging from $X = 1.1$ [m] to $X = 1.4$ [m]. At a later stage at $t_3 = 1.2$ [s] when the wave crest was located above the lee side of the bedform the velocity values decreased in the entire bedform or were even absent in the stoss area. Interestingly, at $t_4 = 1.45$ [s] when the wave had passed the bedform, the measurements showed that the pore water flow direction changed in the upstream X direction. In this case, the inflow velocity values were highest in the region close to the lee side of the bedform from $X = 1.6$ [m] to $X = 1.3$ [m]. Coevally, no pore water flow pattern could be observed in the center part of the bedform whereas low upstream pore water flow occurs along the stoss side. When taking the zoom out at $t_1 = 0.7$ [s] into account (Figure 3E), morphology following vectors combined with low-velocity ranges in the positive X direction become evident. However, when the wave crest had passed the bedform, at $t_4 = 1.45$ [s], the flow infiltrated in the bedform into the negative X direction, which was accompanied by a flow separation zone in which the flow vectors were distributed in a vortex pattern (Figure 3F).

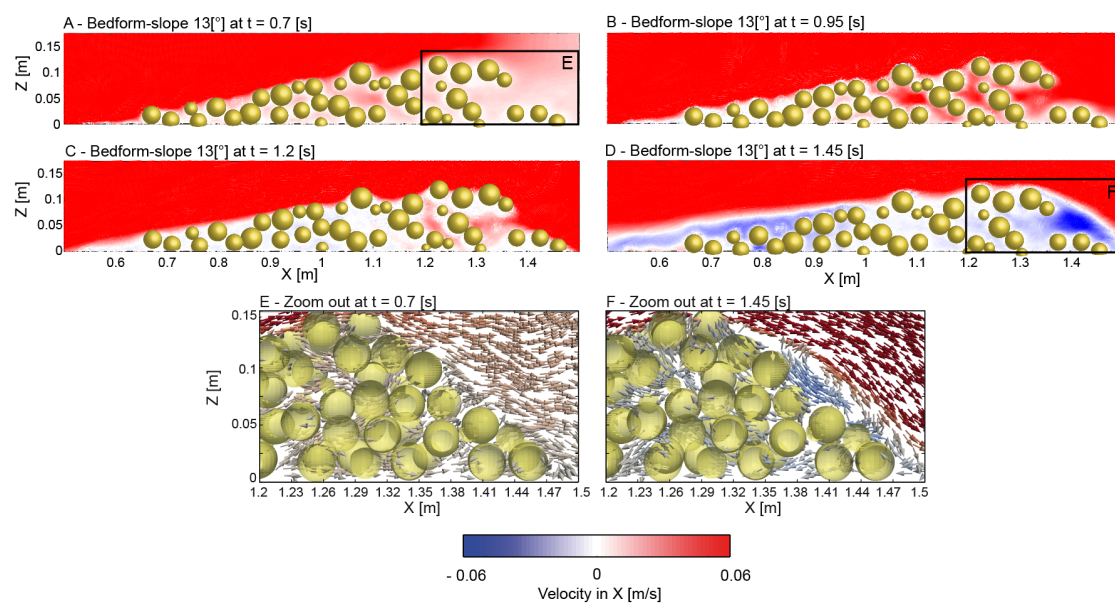


Figure 3. A – D: Overview of the X-Z slices at cut at $Y = 0.11$ [cm], demonstrating fluid inflow into the X direction throughout the pore spaces measured in the interior of each bedform, with respect to wave travel time. The yellow colored spheres indicate the locations of the cut solid particles. E - F: Zoom outs of A and D. The yellow colored spheres in the zoom outs were cut ranging from $Y = 0.9$ [cm] to $Y = 1.2$ [cm] for a better 3D representation.

Pore water flow track lines and flow residence times

The pore water flow track lines processed from the water column reflect the morphology of the bedform (Figure 4). However, those tracks processed from the interior of the bedform indicate a different pattern. The track lines showed that with respect to time an inflow into the bedforms evolved, which resulted in a current flushing throughout the pore spaces into the downstream X direction. Initially, the flow infiltrated the pore spaces at the stoss side of the bedform. Further, the particle track lines indicate that the flow was able to flush through the entire pore space, but appeared most dominant in the region of the steep lee side which is indicated by connected particle track lines ranging from $X = 1.05$ [m] to $X = 1.4$ [m] and $Z = 0.6$ [m] to $Z = 0.15$ [m] (Figure 4A).

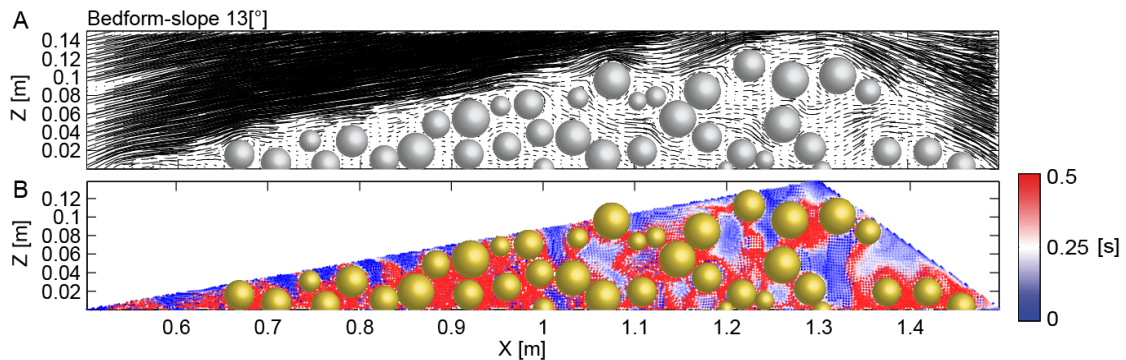


Figure 4. A: Pore water flow track lines, indicating the flow paths from $t_1 = 0.7$ to $t_4 = 1.3$ [s]. The track lines show the flow field in the water column, and in between the pore-spaces. Arrow lengths scale with flow velocities. **B:** Flow residence times, indicating the zones of low and high resisting times ranging from $t_1 = 0.7$ to $t_4 = 1.3$ [s]. The blue color-coded areas indicate zones of low residence times, whereas the red colored areas indicate zones of high residence times. In both figures, the spheres indicate the locations of the cut solid particles.

For the quantification of how long the fluid remained in the pore spaces of the bedform, the residence times are shown in Figure 4. The measurements revealed areas of relatively high (red colors in Figure 4B) and low-residence times (blue colors in Figure 4B) during this solitary wave cycle. When investigating the residence time pattern, the highest residence times were identified predominately within the region of the stoss side in the core of the bedform between $X = 0.0$ [m] and $X = 1.2$ [m] whereas coevally the shallow part of the stoss side is filtrated

Further, lowest residence times are present at the lee side of the bedform between $X = 1.2$ [m] and $X = 1.6$ [m] and below the bedform crest. Interestingly, the distribution of the flow residence time pattern correlates with the particle track lines, which also represents the inflow characteristics into the bed. For example, in the areas where lower residence times were measured, the pore water track lines did show a connected pattern, whereas in the areas with high residence times the pore water track lines were not connected.

DISCUSSION

By the use of a 3D numerical wave tank model, it was possible to simulate a solitary wave flowing over a bedform and to resolve the fluid infiltration into the pore spaces, as well as the flow through the pores. This is supported by the particle tracks and residence times presented in Figure 4. A new conceptual model that highlights our understanding of the hydrodynamic processes that occur above a bedform and in the interior is presented in Figure 5. The conceptual model is based on both former studies ((Baas, 1994; Bartzke et al., 2013; Bennett and Best, 1995; Best, 1992; Best and Kostaschuk, 2002; Black and Paterson, 1997; Heald et al., 2004; Leeder, 1980; Mc Cave, 1984; van Ledden et al., 2004; Venditti and Bennett, 2000; Venditti et al., 2005; Wiberg and Nelson, 1992)), which investigated the hydrodynamic conditions above fixed bedforms and our results that reveal the processes in the interior of bedforms.

When the wave crest was located in front of the bedform (Figure 5), the flow direction appears predominately in the downstream X direction (net flow direction in Figure 5) and is indicated by the black colored fluid profile in Figure 5. In this case the flow pushes against the stoss side and hence forces the water to infiltrate into the pore spaces. As a consequence to this push, a flow into the bedform is initiated that results in a flow throughout the pores spaces, predominately into the downstream direction (black arrows in Figure 5). Interestingly, in this case only the shallow part of the bedform was infiltrated, whereas the pore fluid in the lower sediment portions is more or less at rest. The gray shaded area in Figure 8 indicates the expected zones of highest fluid inflow and flow through the pore spaces. At a later stage, when the wave passed the bedform, the zone of flow separation developed close to the lee side of the bedform (Figure 3E and Figure 5). In consequence, the direction of net flow changes from a predominately downstream direction towards the upstream direction (green fluid profile in Figure 5). As a result, a part of the fluid is pushed in the upstream direction into the pore spaces of the lee side of the bedform. Consequently, the flow direction within the bedform reflects the flow direction in the water column. In addition, inflow depth and the thickness of the infiltrated sediment layer increased at the lee side.

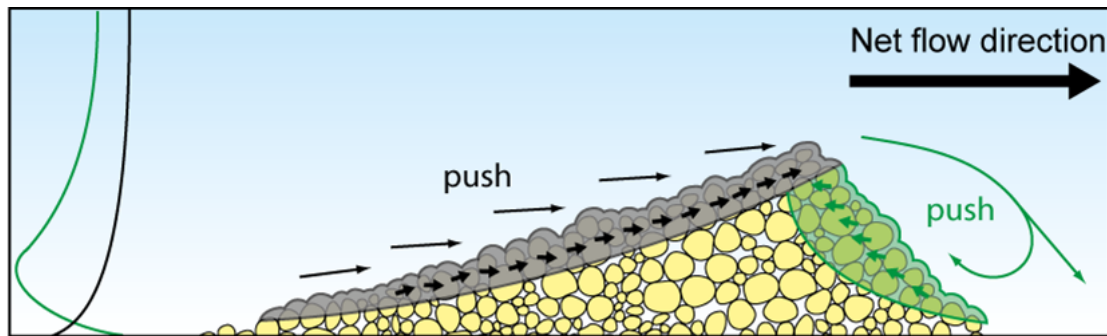


Figure 5. Conceptual model illustrating the hydrodynamic processes in the interior of a flat sloped bedform. The back colored fluid profile indicates the flow condition when the wave crest is located before the bedform, whereas the green colored fluid profile represents the flow condition when the wave crest passed the bedform.

From the hydrodynamic patterns shown in the results section and the conceptual model, it is proposed that the location as well as the amount of inflow might have a significant influence onto the erosion behavior of a bedform. For example in the case of this flat, sloped bedform, it would be expected due to the lower inflow at the stoss side that the stoss side would be more stable, whereas the lee side would presumably be more exposed to erosion due to higher inflow conditions.

Moreover, as many processes in the sedimentary environment depend on pore water inflow, our results can show how inflow into bedforms causes dramatic effects in the interior of a bedform. Our model could help to determine processes that operate in the direct vicinity of the sediment surface and in the interior of bedforms, such as the ease to which chemicals, nutrients, or decaying material are flushed into the water column by pore water flow (Huettel and Webster, 2001; Precht et al., 2004).

CONCLUSION AND OUTLOOK

For the investigation of fluid infiltration into bedforms, a 3D high-resolution numerical tank model was generated using Smooth Particle Hydrodynamics (SPH) as numerical simulation technique. In this framework, the results of a relatively flat bedform having a stoss side slope of 13 [°] are presented. With the objective to quantify the inflow conditions into a bedform a numerical solitary wave was generated by a numerical wave-maker. By this approach, we were able to quantify the hydrodynamic conditions in the water column and simultaneously in the interior of the bedform within the pore spaces. The model results showed that both inflow and flow throughout the pore spaces were evident and appeared highly dependent on the position of the wave crest. This numerical approach allowed the development of an improved conceptual model through the testing of a general hypothesis. The presented conceptual model shows that the locations of inflow and flow direction of the flow in the pore spaces is dependent on the wave crest position.

Following evolution of prior physical experiments, future research will focus on inflow of bedforms, composed of multiple particle size ranges, grain shape variations, as well as on the implementation of moving particles and current flow boundary conditions. The presented findings could help scientists who demand information of the hydrodynamic conditions in the interior of a bedform. Consequently, the results could help to improve the understanding of oxygen enrichment or nutrient supply in the bedform interior. Moreover, the findings could enhance the understanding for bedform erosion and their evolution due to the additional flow that floats throughout the pore spaces, which might potentially modify the threshold conditions for erosion, which will be tested in future experiments.

Any numerical model relies on a number of assumptions and simplifications. Natural grain shapes are irregular and thereby the pore spaces would presumably be smaller. As a result, lower inflow rates as compared to the tested bedforms would be expected. Nevertheless, it is concluded that naturally composed bedforms would show a comparable evolution of the flow characteristics in the pore spaces. As a result, the amount of inflow would be reduced but would be sufficient to enhance erosional processes from the interior of the bedforms. Hence, the presented interpretations clearly need further investigation.

ACKNOWLEDGMENTS

This work has been funded through the DFG Deutsche Forschungs Gemeinschaft and MARUM – Center for Marine Environmental Sciences, Universität Bremen. We thank, Jannis Kuhlmann, Bryna Flaim, and Franziska Staudt.

REFERENCES

- Allen, J. R. L. 1970. *Physical processes of sedimentation*, Unwin University Books, London.
- Baas, J. H. 1994. A flume study on the development and equilibrium morphology of current ripples in very fine sand, *Sedimentology*, 41, 185-209.
- Barreiro, A., A. J. C. Crespo, J. M. Domínguez, and M. Gómez-Gesteira. 2013. Smoothed Particle Hydrodynamics for coastal engineering problems, *Computers & Structures*, 120, 96-106.
- Bartzke, G., K. R. Bryan, C. A. Pilditch, and K. Huhn. 2013. On the Stabilizing Influence of Silt On Sand Beds, *Journal of Sedimentary Research*, 83, 691-703.
- Bennett, S. J., and J. L. Best. 1995. Mean flow and turbulence structure over fixed, two-dimensional dunes: implications for sediment transport and bedform stability, *Sedimentology*, 42, 491-513.
- Best, J. 1992. On the entrainment of sediment and initiation of bed defects: insights from recent developments within turbulent boundary layer research, *Sedimentology*, 39, 797-811.
- Best, J., and R. Kostaschuk. 2002. An experimental study of turbulent flow over a low-angle dune, *Journal of Geophysical Research: Oceans*, 107, 3135.
- Black, K., and D. M. Paterson. 1997. Measurement of the erosion potential of cohesive marine sediment: A review of current in situ technology, *J. Mar Environ. Eng*, 4, 43-83.
- Bridge, J., and R. Demicco. 2008. *Earth Surface Processes, Landforms and Sediment Deposits*, Cambridge University Press.
- Coniglio, M., L. A. Hardie, F. J. Longstaffe, and V. Middleton. 2005. *Encyclopedia of Sediments and Sedimentary Rocks*, Springer.
- Crespo, A., M. Gómez-Gesteira, and R. Dalrymple. 2008. Modeling Dam Break Behavior over a Wet Bed by a SPH Technique, *Journal of Waterway, Port, Coastal, and Ocean Engineering*, 134, 313-320.
- Dalrymple, R. A., and B. D. Rogers. 2006. Numerical modeling of water waves with the SPH method, *Coastal Engineering*, 53, 141-147.
- Drake, T. G., and J. Calantoni. 2001. Discrete particle model for sheet flow sediment transport in the nearshore, *Journal of Geophysical Research: Oceans*, 106, 19859-19868.
- Gomez-Gesteira, M., A. J. C. Crespo, B. D. Rogers, R. A. Dalrymple, J. M. Dominguez, and A. Barreiro. 2012. SPHysics – development of a free-surface fluid solver – Part 2: Efficiency and test cases, *Computers & Geosciences*, 48, 300-307.
- Heald, J., I. McEwan, and S. Tait. 2004. Sediment transport over a flat bed in a unidirectional flow: simulations and validation, *Philos Trans A Math Phys Eng Sci*, 362, 1973-1986.
- Huettel, M., and I. T. Webster. 2001. Porewater flow in permeable sediments, *The benthic boundary layer: transport processes and biogeochemistry*. Oxford University Press, New York, 144-179.
- Julien, P. Y. 1998. *Erosion and Sedimentation*, Cambridge University Press.
- Leeder, M. R. 1980. On the stability of lower stage plane beds and the absence of current ripples in coarse sands, *Journal of the Geological Society*, 137, 423-429.
- Leeder, M. R. 1999. *Sedimentology and Sedimentary Basins: From Turbulence to Tectonics*, Wiley.
- Mc Cave. 1984. Erosion, transport and deposition of fine-grained marine sediments, *Geological Society, London, Special Publications*, 15, 35-69.
- Monaghan, J. J. 1992. Smoothed Particle Hydrodynamics, *Annual Review of Astronomy and Astrophysics*, 30, 543-574.
- Monaghan, J. J. 1994. Simulating Free Surface Flows with SPH, *Journal of Computational Physics*, 110, 399-406.
- Monaghan, J. J. 2005. Smoothed particle hydrodynamics, *Reports on Progress in Physics*, 68, 1703.
- Precht, E., U. Franke, L. Polerecky, and M. Huettel. 2004. Oxygen Dynamics in Permeable Sediments with Wave-Driven Pore Water Exchange, *Limnology and Oceanography*, 49, 693-705.
- Schmeeckle, M. W., and J. M. Nelson. 2003. Direct numerical simulation of bedload transport using a local, dynamic boundary condition, *Sedimentology*, 50, 279-301.
- van Ledden, M., W. G. M. van Kesteren, and J. C. Winterwerp. 2004. A conceptual framework for the erosion behaviour of sand-mud mixtures, *Continental Shelf Research*, 24, 1-11.

- van Rijn, L. C. 1984. Sediment transport, part III: bed forms and alluvial roughness, *Journal of Hydraulic Engineering*, 110, 1733-1754.
- Venditti, J. G. 2013, *9.10 Bedforms in Sand-Bedded Rivers*, in *Treatise on Geomorphology*, edited by J. F. Shroder, San Diego, Academic Press.
- Venditti, J. G., and S. J. Bennett. 2000. Spectral analysis of turbulent flow and suspended sediment transport over fixed dunes, *Journal of Geophysical Research: Oceans*, 105, 22035-22047.
- Venditti, J. G., M. A. Church, and S. J. Bennett. 2005. Bed form initiation from a flat sand bed, *Journal of Geophysical Research: Earth Surface*, 110, F01009.
- Wiberg, P. L., and J. M. Nelson. 1992. Unidirectional flow over asymmetric and symmetric ripples, *Journal of Geophysical Research: Oceans*, 97, 12745-12761.